# Icing detection for small fixed wing UAVs using inflight aerodynamic coefficient estimation

Andreas Wenz *, Tor Arne Johansen*
*Centre for Autonomous Marine Operations and Systems
Department of Engineering Cybernetics
Norwegian University of Science and Technology, Trondheim, Norway

***Abstract*— We propose a method to detect icing of the airfoil of a fixed-wing Unmanned Aerial Vehicle by using an aerodynamic coefficient estimator and ambient temperature and humidity sensors. The estimator uses the information provided by a standard autopilot sensor suite consisting of an IMU, GNSS and a pitot-static tube to estimate lift coefficients as well as steady and turbulent wind velocities. These sensor inputs are fused within an Extended Kalman Filter using frequency separation and kinematic, aerodynamic and wind models while avoiding the need for prior knowledge about the aircraft. Ambient temperature and humidity sensors are used to assess environmental conditions and if icing is suspected, a trigger signal to the estimator and the autopilot is generated. This signal is used to adjust the anticipated uncertainties of the estimated coefficients and, if permitted by the flight control system, to initialize a small altitude change in order to excite the estimator. Simulation results show that this method is able to separate clearly between iced and non-iced cases and can be used to significantly enhance the detection performance compared to only using temperature and humidity based information.**

## I. Introduction

Icing on the wings, propellers, sensors and control surfaces is a major threat to aviation. The build up of ice on the wings can lower the lift and increase the drag significantly. Icing of propellers, sensors, control surfaces and engines can impede their use. The effects of icing and its detection has been studied extensively for manned aviation since the 1940s and is still an active research topic today [6], [5], [9], [13], [11] and has influenced the design of manned aircraft significantly.

Also for unmanned aerial vehicles (UAVs) icing is a serious issue when flying in cold and humid environments. Meteorological studies [3], [4] show that supercooled large drops, which cause inflight icing, appear regularly over large parts of North America, Europe and Asia. These also appear at low altitudes, where small UAVs are typically operated.

The increased drag can lead to a lower energy efficiency and lower the range of the UAV significantly. The decreased lift can cause the autopilot of the UAV to fly at higher angle of attack which in combination with the lower stall angle can result in a high safety risk or in the worst case to a crash of the UAV [12]. These effects of icing can limit UAV operations or prevent them completely, since the typical mitigation for small UAVs is simply to avoid icing.

A general problem when detecting icing on small UAVs is the limited availability of sensor data and a lower level of redundancy compared to manned aircraft. This is due to stricter restrictions concerning size, weight and costs. Previous work therefore focused on icing detection using accurate models of the aircraft dynamics and detecting the changes induced by icing [7], [14], [18]. However in practice for low cost small UAVs it might be difficult to obtain the model parameters to use these methods since these parameters might change from one mission to the other depending on the used payload or due to individual differences in UAV configurations within a fleet of supposedly equal UAVs. Other work [16] required the knowledge of the angle of attack during the flight, which requires the installation of either a multi-hole probe or vanes on the fuselage or trailing edge of the airfoils, or an estimation strategy.

This paper presents a novel approach to icing detection by only using a standard sensor suite, consisting of an inertial measurement unit (IMU), measurements of a global navigation satellite system (GNSS), a pitot-static tube, as well as temperature and humidity sensors. Additionally simple kinematic relationships, a linearized aerodynamic model, and a wind model are used. The needed aerodynamic parameters for these models are estimated online and no prior knowledge of the UAV is needed. By detecting changes in these parameters, airfoil icing can be assessed.

### A. Effects of Icing on Aircraft Aerodynamics

Since airfoil design for UAV follows the same principles as in manned aviation it is reasonable to assume that these airfoils are affected by icing in a similar way. A challenge when applying results from wind tunnel tests for manned aviation to scenarios with small fixed wing UAVs is that the wind velocity profiles used in the wind tunnel test are adjusted to the cruising speeds of the regarded aircraft. The airspeed, which affect the ice accretion significantly, is much lower for the small unmanned aircrafts and might result in different ice types and shapes.

Ratvasky et.al. [13] describe inflight icing as a consequence of flying through clouds containing super-cooled liquid droplets which hit the surface of the aircraft. Depending on atmospheric environment parameters, the flight condition, the geometry of the aircraft and time in icing conditions the ice can accumulate in different shapes which affect the flight performance differently. The atmospheric environment around the aircraft is commonly described by three parameters:

- Liquid Water Content (LWC): a measure of the amount of liquid water in a unit volume of space.
- Median Volumetric Diameter (MVD): describes spectrum of the volume of the incoming droplets, where the 50 % of droplets have a smaller volume and 50 % have a larger volume
- Static Temperature ($T_s$): the ambient air temperature.

A study by Bragg et.al. [5] shows how these parameters result in different kinds of icing and how these affect the aerodynamic parameters of the UAV. The four different described icing types are "Streamwise", "Horn", "Spanwise Ridge" and "Roughness". Depending on the type of icing the maximum lift, the stall angle and the linear lift coefficient are reduced. Parasite drag can be increased by over $400\%$. The Reynolds number of the regarded subscale airfoil is one order of magnitude higher than the Reynolds number of small UAVs studied in this paper. [8] shows that similar effects of icing can be observed at low Reynolds numbers typical for small UAVs.

### B. Contribution of the Paper

This paper builds up on [19] which presents a method to estimate wind velocities and aerodynamic coefficients using a standard sensor suite consisting of an IMU, a GNSS receiver and a pitot-static tube. In simulations it was shown that the proposed estimator after an initialization phase provides accurate estimates of the aerodynamic coefficients and the wind velocities. Using these, estimates of the angle of attack, the sideslip angle and the airspeed can be calculated.
In [19] it was assumed that the aerodynamic coefficients are constant. The main contribution of this paper is to apply the estimator to the case where this assumption does not hold, namely in icing conditions. This can be achieved by increasing the anticipated uncertainties within the estimator and triggering an altitude change, when icing is suspected based on the measured ambient temperature and humidity. This results in an icing detection architecture which is able to discriminate between icing and non-icing conditions without the need of prior knowledge about the aircraft or additional sensors other than the standard autopilot sensor suite and a temperature and humidity sensor.

## II. Icing Detection Architecture

The ice detection architecture is designed to detect changes in the lift coefficients of the airfoil. Maximum lift and stall angle are typically significantly influenced by icing. However since it is undesirable to get into stall conditions during flight it is challenging to detect changes within these parameters. One approach might be to estimate the drag coefficient, which changes significantly during icing [5], using the pitot-static tube and the accelerometer measurements. However this is challenging since these variables are dependent on the engine thrust and control surface deflections and their respective parameters, which are usually not accurately measured and also influenced by icing.
On the other side [5], [8] also shows that the lift coefficient increases less with increasing angle of attack when affected by icing. In a lift force model this is described by the linear lift coefficient $C_{L,\alpha}$. The change in $C_{L,\alpha}$ appears already at low angles of attack ($\alpha$) and can be detected without risking wing stall of the aircraft.

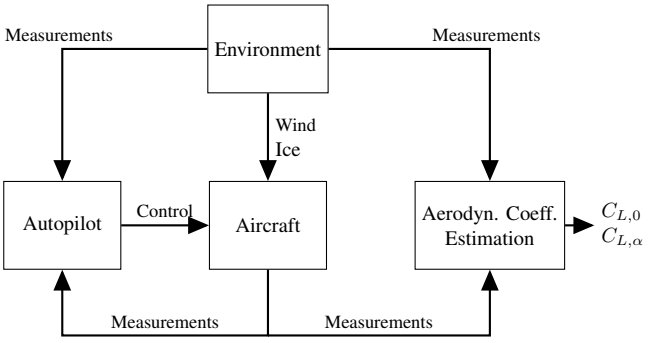

Fig. 1: Icing detection structure

Figure 1 shows the proposed structure of the icing detector. The aircraft is affected by its environment, where some of the major influences are wind and ice. A temperature and humidity sensor is used to assess the current environmental conditions. If these exceed a threshold, icing is suspected and a trigger signal is send to the autopilot, which steers the UAV, and to an aerodynamic coefficient estimator. The trigger signal is used to adjust the estimated uncertainties within the estimator to the current conditions and to the autopilot for necessary excitation of the estimation, if admissible from the flight management system.

## III. Aerodynamic coefficient estimator

The used aerodynamic coefficient estimator was first presented in [19]. It uses kinematic and aerodynamic relationships as well as a wind model to estimate wind velocities and aerodynamic coefficients from the pitot-static tube, accelerometers and velocities over ground measured by a Global Navigation Satellite System (GNSS). Additionally an estimate of the rotation matrix from navigation to body frame $\boldsymbol{R}_n^b$ is needed from an Attitude and Heading Reference System (AHRS). As an estimator the Extended Kalman Filter (EKF) [15] is used. An overview on the structure of the estimator is shown in Figure 2. The estimation will be shortly described, and for a more detailed description see [19].

### A. Aerodynamic Model

The estimator uses a simplified model of the aerodynamics in the z-direction of the body frame:

$$f_z = a_z - g\cos(\theta)\cos(\phi) \tag{1}$$
$$= KV_a^2\left(C_{L,0} + \alpha C_{L,\alpha}\right) \tag{2}$$

where $a_z$ is the z-accelerometer measurement and $f_z$ is the aerodynamic acceleration in z-direction, $g$ is the gravitation constant and $\theta, \phi$ are the pitch and roll angle. $K = \frac{\rho S}{2m}$ is a constant factor consisting of the air density $\rho$, the wing area $S$ and the mass of the aircraft $m$. $C_{L,0}$ is the constant lift coefficient and $C_{L,\alpha}$ is the linear lift coefficient. We assume that accelerometer biases are estimated in the AHRS so that

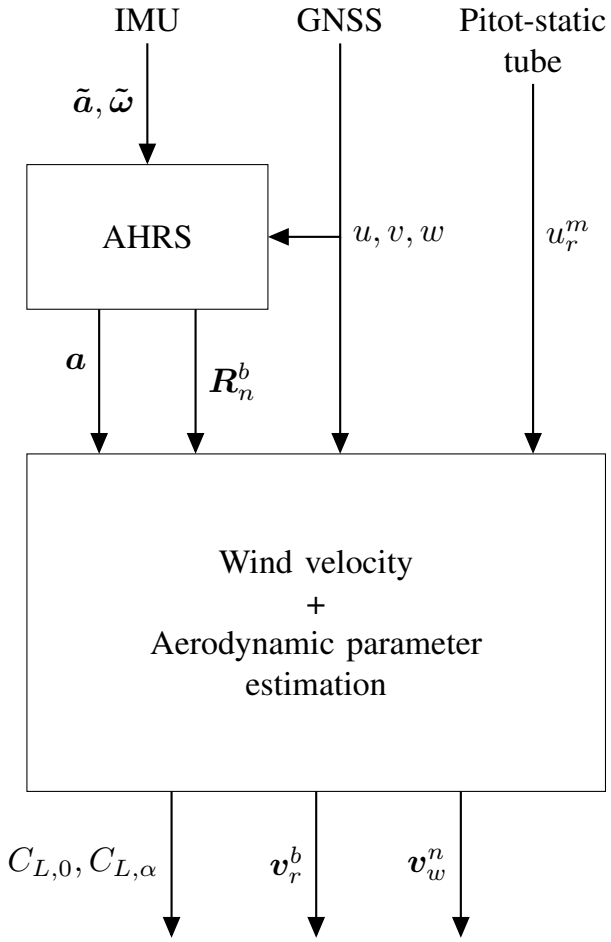


Fig. 2: Estimation structure

$a_z$ is bias-free. This model neglects the influence of forces induced by drag, the pitch rate and the elevator deflection, which are typically at least 1 orders of magnitude smaller than the influence of the lift force at small angles of attack. $V_a$ is the airspeed and $\alpha$ is the angle of attack which are defined as:

$$\alpha = tan^{-1}\left(\frac{w_r^b}{u_r^b}\right) \tag{3}$$

$$V_a = \|\boldsymbol{v}_r^b\| \tag{4}$$

Here $\boldsymbol{v}_r^b = (u_r^b v_r^b w_r^b)^T$ is the velocity of the aircraft relative to the surrounding airmass decomposed in body frame which is given by the wind triangle:

$$\boldsymbol{v}_r^b = \boldsymbol{v}^b - \boldsymbol{R}_n^b \boldsymbol{v}_w^n \tag{5}$$

$$\boldsymbol{v}^b = \boldsymbol{R}_n^b v^n \tag{6}$$

Where $\boldsymbol{v}^n = (u, v, w)$ is the velocity over ground and $v_w^n$ is the local wind velocity over ground, decomposed in NED frame. In (5)-(6) the variables $u_r^b$, $\boldsymbol{v}^n$ and $R_n^b$ are given, the wind velocity $\boldsymbol{v}_w^n$ needs to be estimated in order to obtain the full vector $\boldsymbol{v}_r^b$. This is important for small UAVs since the wind speed may be of similar magnitude as the airspeed. This model of the aerodynamics in z-direction is simplified and neglects the effects of drag on the body z-acceleration and linearizes the underlying trigonometric functions. However, for small angles of attack and non-stall conditions the model errors induced by this simplifications are small and do not degrade the estimation performance.

### B. Wind Model

In the following we use a time-discrete model where $k$ denotes the current time index and $\Delta x_k$ the difference between $x_k$ and $x_{k-1}$. We assume the wind velocity $\boldsymbol{v}_w^n$ to have two parts. A low-frequent steady part $\boldsymbol{v}_s^n$ and a high-frequent turbulent part $v_t^n$ which are governed by the following discrete dynamics: [2, pp.55].

$$\boldsymbol{v}_{w,k}^n = \boldsymbol{v}_{s,k}^n + \boldsymbol{v}_{t,k}^n \tag{7}$$

$$\Delta \boldsymbol{v}_{s,k}^n \approx 0 \tag{8}$$

$$\Delta \boldsymbol{v}_{t,k}^n = -\Delta T V_{a,k} \begin{pmatrix} \frac{u_t^n}{L_u} \\ \frac{v_t^n}{L_v} \\ \frac{w_t^n}{L_w} \end{pmatrix}\Bigg|_k + \begin{pmatrix} \sigma_u \sqrt{2\Delta T \frac{V_a}{L_u}} \eta_u \\ \sigma_v \sqrt{2\Delta T \frac{V_a}{L_v}} \eta_v \\ \sigma_w \sqrt{2\Delta T \frac{V_a}{L_w}} \eta_w \end{pmatrix}\Bigg|_k \tag{9}$$

The dynamic equations for the turbulent wind velocity (9) are known as the Dryden wind model [1]. The spatial wavelengths $L_x$ are given by:

$$L_{u,k} = L_{v,k} = \frac{h_k}{(0.177 + 0.000823 \cdot h_k)^{1.2}} \tag{10}$$

$$L_{w,k} = h_k \tag{11}$$

where $h_k$ is the current altitude above ground. The random white noise amplitudes are given by:

$$\sigma_{u,k} = \sigma_{v,k} = V_{w,G} \frac{0.1}{(0.177 + 0.000823 \cdot h_k)^{0.4}} \tag{12}$$

$$\sigma_w = 0.1 \cdot V_{w,G} \tag{13}$$

where $V_{w,G}$ is the wind speed measured 6 meters above ground.

### C. Estimation Setup

Because of the non-linear nature of the model, an Extended Kalman Filter (EKF) is used as an estimator. The states to be estimated are the steady and the turbulent wind velocities decomposed in NED frame, the two lift coefficients and a scaling factor governing pitot-static tube calibration, (cf. (19)):

$$\boldsymbol{x} = \begin{bmatrix} u_s^n & v_s^n & w_s^n & u_t^n & v_t^n & w_t^n & C_{L_0} & C_{L_\alpha} & \gamma \end{bmatrix}^T \tag{14}$$

The state transition matrix for the prediction step of the EKF are given by:

$$\begin{aligned} \boldsymbol{x}_{k|k-1} =& \boldsymbol{f}(\boldsymbol{x}_{k-1|k-1}) \\ =& \boldsymbol{x}_{k-1|k-1} + \begin{bmatrix} 0 & 0 & 0 & \Delta v_{t,k-1} & 0 & 0 & 0 \end{bmatrix}^T \end{aligned} \tag{15}$$

Where

$$\Delta \boldsymbol{v}^n_{t,k-1} = -\bar{V}_a \Delta T \left( \begin{matrix} \frac{u_t}{L_u} \\ \frac{v_t}{L_v} \\ \frac{w_t}{L_w} \end{matrix} \right) \Bigg|_{\substack{\boldsymbol{u}_{k-1} \\ \boldsymbol{x}_{k-1|k-1}}} \tag{16}$$

$\bar{V}_a$ is a low-frequency version of $V_a$ which is only dependent on the velocity over ground $\boldsymbol{v}^b$, and the steady wind velocity $\boldsymbol{v}^n_s$ and independent of the turbulent wind velocity $\boldsymbol{v}^n_t$.

$$\bar{V}_a = \left\| \boldsymbol{v}^b - \boldsymbol{R}^b_n \boldsymbol{v}^n_s \right\| \tag{17}$$

The underlying assumption made in (16) is that, when predicting the turbulent wind velocity, the airspeed, and thous the response of the Dryden low pass filter, can be regarded as independent of the turbulent wind velocity. Measurements for correcting the state vector are the aerodynamic acceleration in z-direction in body frame $f_z$ and the longitudinal velocity over ground decomposed in body frame $u^b$.

$$\boldsymbol{z}_k = \begin{bmatrix} f_z \\ u^b \end{bmatrix} = \begin{bmatrix} a_z - g\cos(\theta)\cos(\phi) \\ u^b \end{bmatrix} + \boldsymbol{\nu}_k \tag{18}$$

where $g$ is the local gravity of Earth, $\theta, \phi$ are the pitch and roll angles and $\nu$ is some measurement noise. The time varying measurement function is given by:

$$\begin{aligned} \boldsymbol{h}(\boldsymbol{x}, \boldsymbol{u}) &= \begin{bmatrix} -K\bar{V}_a^2 (C_{L_0} + C_{L_\alpha}\alpha) \\ \boldsymbol{d}_1^T \boldsymbol{R}^b_n (\boldsymbol{v}^n_s + \boldsymbol{v}^n_t) + \gamma u^m_r \end{bmatrix} \\ \boldsymbol{d}_1^T &= \begin{bmatrix} 1 & 0 & 0 \end{bmatrix} \end{aligned} \tag{19}$$

The first measurement equation in (19) uses the aerodynamic model (2) to estimate the aerodynamic coefficients and the wind velocities via $\bar{V}_a$ and $\alpha$. Here $\bar{V}_a$ is used to interpret fast changes in the acceleration $f_z$ as to be induced by changes in the angle of attack $\alpha$, which has higher frequency components, and not by changes in the airspeed due to turbulence. This assumption provides different gradients when differentiating (19) with respect to $\boldsymbol{v}^n_s$ and $\boldsymbol{v}^n_t$ and therefore allows separate observation of these states. The second measurement equation utilizes the wind triangle (5) to relate the measurements of the velocity over ground to the relative longitudinal velocity $u^m_r$ measured by the pitot-static tube. This is similar to the method described in [10].

### D. Handling Uncertainty in Icing Conditions

In an EKF the uncertainty of the state estimate is estimated by the covariance matrix estimate $\boldsymbol{P}$, which is initialized with a matrix $\boldsymbol{P}_0$. The uncertainty from process noise and modeling errors is described by a covariance matrix $Q$ which is defined as:

$$\boldsymbol{Q}_k = diag \begin{pmatrix} a_{u^n_s} \\ a_{v^n_s} \\ a_{w^n_s} \\ a_{u^n_t}\sigma_{u,k}\sqrt{2\Delta T \frac{\bar{V}_{a,k}}{L_{u,k}}} \\ a_{v^n_t}\sigma_{v,k}\sqrt{2\Delta T \frac{\bar{V}_{a,k}}{L_{v,k}}} \\ a_{w^n_t}\sigma_{v,k}\sqrt{2\Delta T \frac{\bar{V}_{a,k}}{L_{w,k}}} \\ a_{C_{L,0}} \\ a_{C_{L,\alpha}} \\ a_\gamma \end{pmatrix} \Delta T^2 \tag{20}$$

where the $a_i$ are tuning parameters. In [19] it was shown in simulations that attitude changes are necessary during filter initialization to achieve good estimates of the aerodynamic coefficients and from time to time afterwards to avoid drift of the estimates. This is true for the case when the coefficients $C_{L,0}$ and $C_{L,\alpha}$ are constant. In this case the covariance parameters associated with these coefficients can be chosen to low values in order to lower the need for corrections during the estimation. However as has been discussed in section I-A, in icing conditions these coefficients are likely to change during the flight. Choosing larger values of the tuning parameters $a_{C_{L,0}}$ and $a_{C_{L,\alpha}}$ would require a high frequency of attitude changes to monitor the coefficients. To avoid this, the information of the temperature and humidity sensors are used. If the ambient temperature is below a certain threshold $T_{crit}$ and the humidity is above a threshold $H_{crit}$ the covariance associated with the change in lift coefficients within the estimator is increased by setting the elements covariance matrix $\boldsymbol{P}$ corresponding to the coefficients to predefined values. Simultaneously a small altitude change $\delta h$ is commanded to the autopilot which if permitted results in a change in pitch angle. The instant rise in estimated uncertainty ensures a fast detection of changes in the aerodynamic parameters while minimizing additional maneuvering. This procedure would have to be repeated if icing conditions are suspected to change.

## IV. Simulation Setup

### A. UAV simulation

All simulations were performed using a simulation of the X8 flying wing and a simulated autopilot. The simulator and the autopilot are based on Beard and McLain [2, Chap. 4 and 6] and implemented in Matlab / Simulink. In the aircraft simulation a more complex non-linear model of the aerodynamics is used (for details see [2, pp.44]). The aerodynamic forces are thus given by:

$$\zeta = \frac{1 + e^{-M(\alpha-\alpha_0)} + e^{M(\alpha+\alpha_0)}}{\left(1 + e^{-M(\alpha-\alpha_0)}\right)\left(1 + e^{M(\alpha+\alpha_0)}\right)} \tag{21}$$

$$\begin{aligned} C_L(\alpha) =& (1-\zeta)(C_{L,0} + C_{L,\alpha}\alpha) + \\ & \zeta(2\,\mathrm{sign}(\alpha)\sin(\alpha)^2\cos(\alpha)) \end{aligned} \tag{22}$$

$$F_L = \frac{1}{2}\rho V_a^2 S (C_L(\alpha) + C_{L,q} c/(2V_a) q + C_{L,\delta_e}\delta_e) \tag{23}$$

$$\begin{aligned} C_{D,\alpha} =& C_{D,p} + (1-\zeta)\frac{(C_{L,0} + C_{L,\alpha}\alpha)^2}{\pi e (b^2/S)} + \\ & \zeta 2\,\mathrm{sign}(\alpha)\sin(\alpha)^3 \end{aligned} \tag{24}$$

$$\begin{aligned} F_D =& \frac{1}{2}\rho V_a^2 S \\ & \left( C_{D,\alpha} + C_{D,q}\frac{c}{2V_a} q + C_{D,\delta_e}|\delta_e| \right) \end{aligned} \tag{25}$$

$$\begin{pmatrix} f_x \\ f_z \end{pmatrix} = \begin{pmatrix} \cos\alpha & -\sin\alpha \\ \sin\alpha & \cos\alpha \end{pmatrix} \begin{pmatrix} -F_D/m \\ -F_L/m \end{pmatrix} \tag{26}$$

where $M$ and $\alpha_0$ are positive constants, $c$ is the mean aerodynamic chord of the wing, $q$ is the pitch-rate and $\delta_e$ is the elevator deflection and $C_{L,q}, C_{L,\delta_e}, C_{D,q}, C_{D,\delta_e}$ are

their respective lift and drag coefficients.
Wind velocity is simulated following Beard and McLain [2, pp.55] as the sum of a steady and a turbulent wind velocity component, where the turbulence is generated by passing white noise through a low pass filter. The filter is designed in the way described in section III-B according to the Dryden model. The steady wind velocity and the wind velocity at 6m above ground, used for the turbulence generation, were set to $6m/s$, the wind direction was set to $90°$.

### B. Simulation of Icing

Icing is simulated using the results from wind tunnel tests discussed in section I-A. In [8] icing was simulated in a wind tunnel on swept wing models with Reynolds numbers between $3 \cdot 10^5$ and $7.8 \cdot 10^5$. The X8 flying wing regarded in this paper has a Reynolds number of $4.5 \cdot 10^5$ and therefore we are assuming that icing effects the X8 similarly. During a period of $100s$ the linear lift coefficient $C_{L,\alpha}$ is reduced by $20\%$ and $\alpha_0$ by $20\%$. This results in a reduction of $C_{L,max}$ by $22\%$ and of the stall angle by $2.9°$. Figure 3 shows the simulated lift coefficient for different angles of attack in the iced and non-iced case. In the same period the drag coefficient is increased by $200\%$.

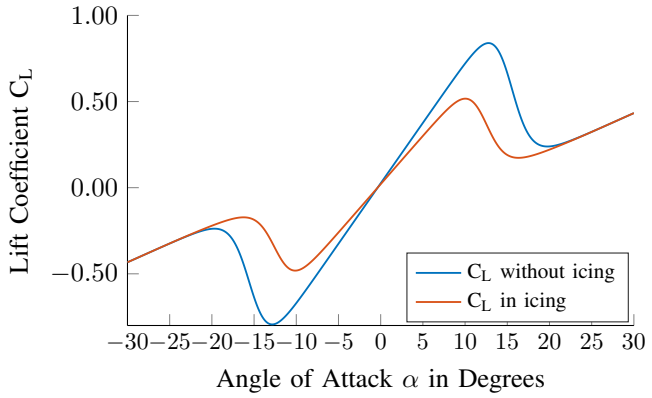


Fig. 3: Lift coefficient vs. angle of attack for iced and non-iced case

### C. Tuning and Initial Conditions

The initial condition for the state vector estimate was set to:

$$\boldsymbol{x}_0 = \begin{bmatrix} 0 & 0 & 0 & 0 & 0 & 0 & 0 & 1 & 1 \end{bmatrix}^T \tag{27}$$

The inital condition for the state covariance matrix was set to:

$$\boldsymbol{P}_0 = diag \begin{bmatrix} 10^{-2} & 10^{-2} & 10^{-4} & 10^{-5} & 10^{-5} \\ 10^{-5} & 10^{-5} & 10^{-1} & 10^{-8} \end{bmatrix} \tag{28}$$

The tuning parameters of the process noise covariance matrix $\boldsymbol{Q}$ were set to:

$$a = \begin{bmatrix} 10^{-7} & 10^{-7} & 10^{-10} & 5 \cdot 10^2 & 5 \cdot 10^2 \\ 2 \cdot 10^2 & 10^{-6} & 10^{-16} & 10^{-15} \end{bmatrix} \tag{29}$$

Notice that the tuning parameter for $C_{L,\alpha}$ was set to a low value to achieve quick convergence after the covariance reset and a small drift when the coefficient is constant. The covariance matrix of the measurement noise was chosen to:

$$\boldsymbol{R} = \begin{bmatrix} 1 & 0 \\ 0 & 0.6 \end{bmatrix} \tag{30}$$

This covariance matrix is important in tuning the EKF. It quantifies the expected uncertainties in the measurement equation induced by noise in the sensors and errors within the attitude estimation. The measurement noise $\nu$, which disturbs the GNSS and the accelerometer measurements, is modeled as band limited white noise with the following standard variances:

$$\sigma_\nu = \begin{bmatrix} 10^{-1} m^2/s^4 \\ 10^{-3} m^2/s^2 \end{bmatrix} \tag{31}$$

Additionally the pitot-tube measurement is affected by band limited white noise with a variance of $0.1m^2/s^2$. It was assumed in the simulation that the AHRS system supplies the estimator with accurate attitude angles with negligible noise levels.

### D. Simulated Scenario

We simulate a takeoff and some loitering, which is often performed in UAV missions by the safety pilot before handing control over to the autopilot. These are important for convergence of the estimator. The commanded altitude is $150m$ and the commanded course angle is $60°$. The UAV performs one circle per minute during the initial period.
At time $300s$ the icing starts and the model coefficients change linearly within $100s$ to their icing values. At time $400s$ the trigger signal is set which leads to a reset of the covariance matrix. The new values are

$$P_{C_{L,0}} = P_{(7,7)} = 10^{-5} \tag{32}$$

$$P_{C_{L,\alpha}} = P_{(8,8)} = 10^{-3} \tag{33}$$

Since no change in $C_{L,0}$ is expected a lower covariance value is chosen to reduce the estimated uncertainty within the $C_{L,0}$ estimate. Simultaneously an altitude change of $20m$ for $50s$ is commanded. Later the UAV changes altitude again to $250m$ and course $20°$ at two different time instants. At the altitude changes during icing the climb rate is limited so that the angle of attack stays well below the stall angle. The input signals can be seen in Figure 4 and Figure 5.

## V. Simulation Results

### A. Aerodynamic Coefficient Estimates

Figure 6 shows the estimates of the lift coefficients and their true values over time. Both coefficients converge quickly to an interval relatively close to their true values after takeoff. When icing occurs their is first no significant change within the lift coefficients. After the covariance reset the $C_{L,\alpha}$ estimate converges quickly close to the new reference values in icing. Afterwards some parameter drift occurs which is due to the increased uncertainty. The altitude and course changes at $600s$ cause additional excitations of the estimator which decrease the uncertainty and compensate the drift somewhat. The drift in $C_{L,\alpha}$ also results in a drift in $C_{L,0}$ which compensates the error induced into the

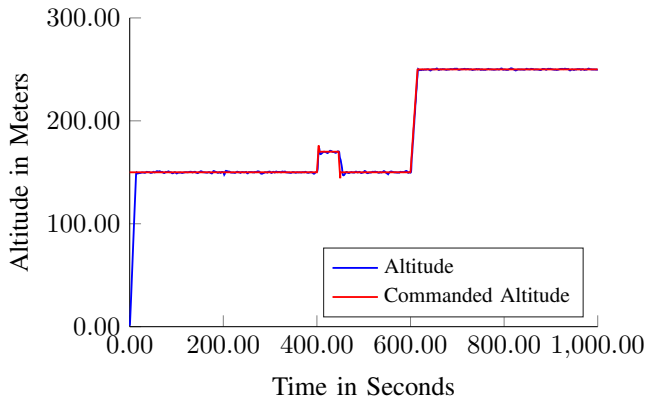


Fig. 4: Commanded and resulting altitude of the UAV

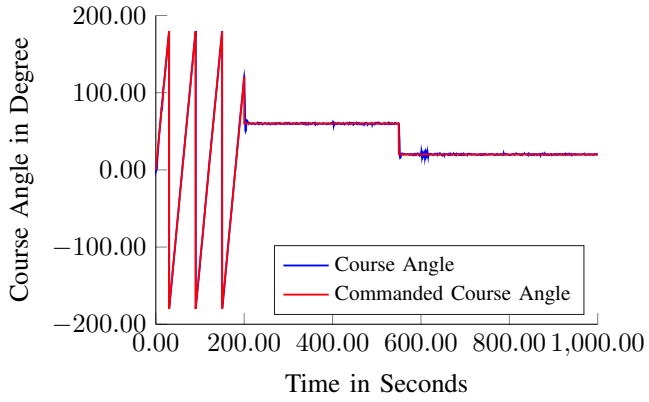


Fig. 5: Commanded and resulting course angle of the UAV

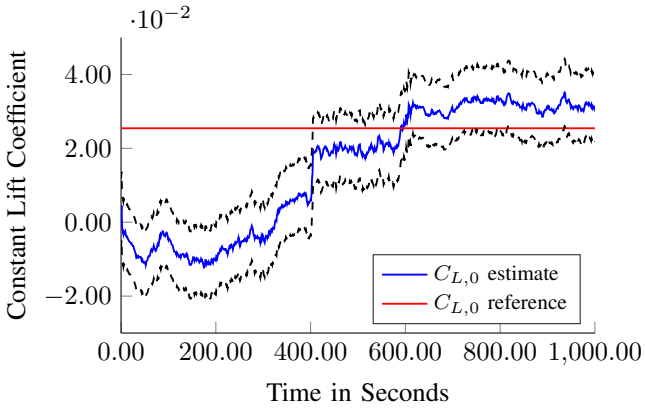


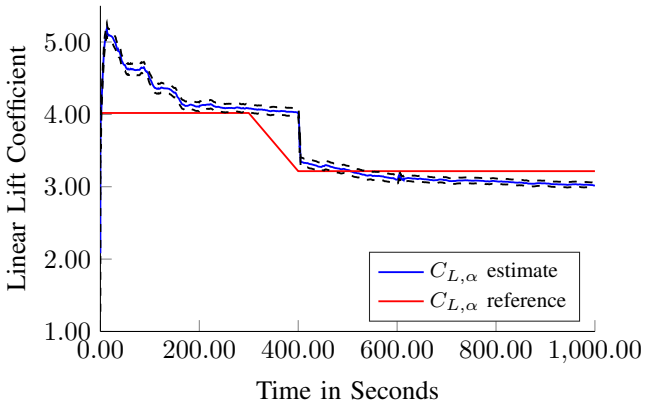


Fig. 6: Estimates and reference of static and linear lift coefficient, icing starts at $300s$, dashed black lines indicate 3 $\sigma$ intervall

measurement equation (19). For comparison Figure 7 shows the estimate of $C_{L,\alpha}$ in the same scenario without icing. This shows that the here proposed icing detector is able to separate clearly between the iced and non-iced case.
Note that a change in pitch angle is necessary to gain information on the wind velocity in down direction, this enables the estimator to distinguish between changes in wind velocity and changes in lift coefficients. This means that for a continuous monitoring of wing icing the covariance reset followed by a change in pitch angle has to be repeated periodically when environmental conditions suggest icing (i.e. humidity increase when flying through clouds). A way to overcome the necessity of these attitude changes might be the installation of a second pitot-static tube in the aircraft pointing downwards or upwards, what makes it possible to measure the relative velocity in down direction directly.

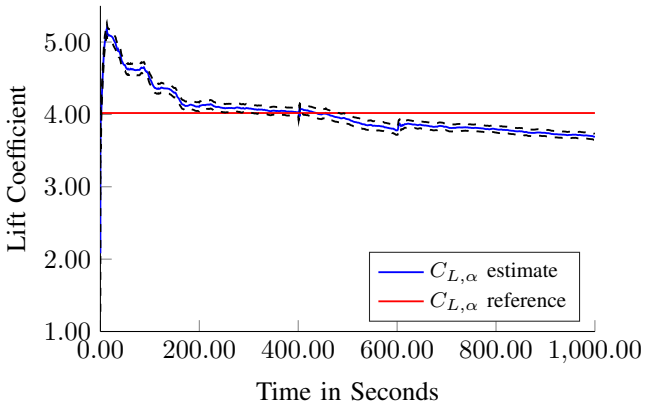


Fig. 7: Estimates and reference of linear lift coefficient without icing, dashed black lines indicate $3\sigma$ intervall

### *B. Airspeed and Angle of Attack Estimates*

Figure 8 shows the estimate of the airspeed during the icing detection. The estimator is able to provide a reliable airspeed estimate during the whole flight. The increased airspeed at $400s$ and $600s$ is caused by the altitude changes. Notably the estimation also performs well at that instance. Equation (2) can be used to calculate $\alpha$ using the airspeed estimate as well as the aerodynamic coefficient estimates and the z-acceleration. Figure 9 shows the resulting $\alpha$ estimate. This estimate is performing well during most of the flight. During the time between $T = 300s$ and $T = 400s$ when the icing is not yet detected the $\alpha$ is less accurate due to a not adapted $C_{L,\alpha}$ estimate. However it is performing well during the altitude changes where higher and lower angles of attack occur ($T = 400s$ and $T = 600s$) and the lift coefficients are estimated correctly again. This could be used to assess flight performance and safety during icing conditions. Additionally this information could be used to limit the allowed flight

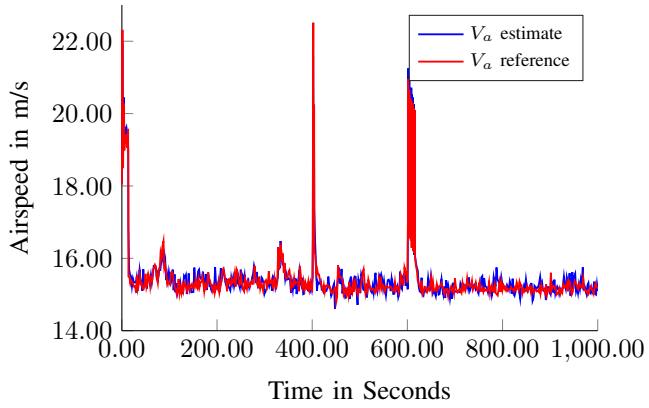


Fig. 8: Airspeed estimate (blue), reference (red)

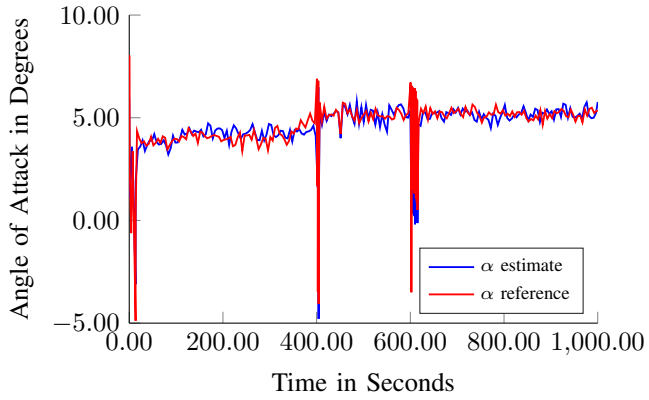


Fig. 9: Angle of Attack estimation(blue), reference (red)

envelope, in particular climb rate of the autopilot in order to reduce the risk of wing stall.

## VI. Conclusion

This paper studies the application of an aerodynamic lift coefficient estimator to the problem of detecting in-flight icing of small fixed wing UAVs. In addition to a standard autopilot suite it uses sensors for temperature and humidity which sends a trigger signal to the estimator if icing is suspected. This enables a partial covariance matrix reset, which suggests an increased uncertainty in the linear lift coefficient estimate. Simultaneously an altitude change is performed which excites the estimator and leads to a quick convergence of the estimate to its true value.
If icing has occurred the value of the linear lift coefficient will be lower than in non-icing conditions and thous can be used as a valuable icing indicator for a deicing system [17]

## VII. Acknowledgments

This project has received funding from the European Unions Horizon 2020 research and innovation programme under the Marie Sklodowska-Curie grant agreement No 642153. The research was also funded by the Research Council of Norway through the Centres of Excellence funding scheme, grant number 223254 NTNU AMOS.
We would like to thank Kristoffer Gryte for the development of the UAV simulator.

## References

[1] MIL-STD-1797A: Flying Qualities of Piloted Aircraft. Technical report, 2004.
[2] Randal W. Beard and Timothy W. McLain. *Small Unmanned Aircraft: Theory and Practice*. Princeton University Press, 2012.
[3] Ben C. Bernstein and Christine Le Bot. An inferred climatology of icing conditions aloft, including supercooled large drops. Part II: Europe, Asia, and the Globe. *J. Appl. Meteorol. Climatol.*, 48(8):1503–1526, 2009.
[4] Ben C. Bernstein, Cory A. Wolff, and Frank McDonough. An Inferred Climatology of Icing Conditions Aloft, Including Supercooled Large Drops. Part I: Canada and the Continental United States. *J. Appl. Meteorol. Climatol.*, 46(11):1857–1878, 2007.
[5] M Bragg, A Broeren, H Addy, M Potapczuk, D Guffond, and E Montreuil. Airfoil Ice-Accretion Aerodynamics Simulation. In *AIAA Aerosp. Sci. Meet. Exhib.*, volume 85, pages 1–22, Reno, Nevada, 2007.
[6] M B Bragg, T Hutchinson, J Merret, R Oltman, and D Pokhariyal. Effect of Ice Accretion on Aircraft Flight Dynamics. In *AIAA Aerosp. Sci. Meet. Exhib.*, volume 2000-0360, 2012.
[7] Andrea Cristofaro, Tor Arne Johansen, and Pedro Aguiar. Icing Detection and Identification for Unmanned Aerial Vehicles : Multiple Model Adaptive Estimation. In *Eur. Control Conf.*, 2015.
[8] J.M. Diebold, M.C. Monastero, and M B Bragg. Aerodynamics of a swept wing with leading-edge ice at low Reynolds number. In *AIAA Appl. Aerodyn. Conf.*, New Orleans, Louisiana, 2012.
[9] R. W. Gent, N. P. Dart, and J. T. Cansdale. Aircraft icing. *Philos. Trans. R. Soc. A Math. Phys. Eng. Sci.*, 358(1776):2873–2911, 2000.
[10] Tor A Johansen, Andrea Cristofaro, Kim Sørensen, Jakob M Hansen, and Thor I Fossen. On estimation of wind velocity , angle-of-attack and sideslip angle of small UAVs using standard sensors. In *Int. Conf. Unmanned Aircr. Syst.*, Denver, 2015.
[11] Terry K. Michie. Airborne weather radar system with icing detection capabiliy, jan 1996.
[12] D Pokhariyal, M B Bragg, T Hutchison, and J Merret. Aircraft Flight Dynamics with Simulated Ice Accretion. *AIAA Aerosp. Sci. Meet. Exhib.*, 2001.
[13] Thomas P Ratvasky, Billy P Barnhart, and Sam Lee. Current Methods for Modeling and Simulating Icing Effects on Aircraft Performance , Stability and Control. *J. Aircr.*, 47.1(1):201–211, 2010.
[14] Damiano Rotondo, Andrea Cristofaro, Tor Arne Johansen, Fatiha Nejjari, and Vicenc Puig. Icing detection in unmanned aerial vehicles with longitudinal motion using an LPV unknown input observer. In *IEEE Conf. Control Appl.*, 2015.
[15] Dan Simon. Nonlinear Kalman filtering. In *Optim. State Estim.*, pages 393–431. John Wiley & Sons, Inc., 2006.
[16] Kim Lynge Sørensen, Mogens Blanke, and Tor Arne Johansen. Diagnosis of Wing Icing Through Lift and Drag Coefficient Change Detection for Small Unmanned Aircraft. In *9th IFAC Symp. Fault Detect. Superv. Saf. Tech. Process.*, number 223254, 2015.
[17] Kim Lynge Sørensen, Andreas Strand Helland, and Tor Arne Johansen. Carbon nanomaterial-based wing temperature control system for in-flight anti-icing and de-icing of unmanned aerial vehicles. In *IEEE Aerosp. Conf. Proc.*, pages 1–6, Big Sky, Montana, 2015.
[18] M. M. Tousi and K. Khorasani. Robust observer-based fault diagnosis for an unmanned aerial vehicle. In *2011 IEEE Int. Syst. Conf.*, pages 428–434. IEEE, apr 2011.
[19] Andreas Wenz, Tor Arne Johansen, and Andrea Cristofaro. Combining model-free and model-based Angle of Attack estimation for small fixed-wing UAVs using a standard sensor suite. In *Int. Conf. Unmanned Aircr. Syst.*, Arlington, VA, 2016.